Isobaric molecular dynamics simulations of hard sphere systems

T. Gruhn and P. A. Monson
Department of Chemical Engineering, University of Massachusetts, Amherst, Massachusetts 01003
(Received 18 January 2001; published 23 May 2001)

We describe an implementation of the Andersen algorithm for simulating the molecular dynamics in the isobaric isoenthalpic (NPH) ensemble for the hard sphere potential. The work is based on the adaptation of the Andersen algorithm to hard spheres by de Smedt *et al.* For a hard sphere system in the NPH ensemble, the particle velocities are not constant between collisions and we describe an efficient method for handling this part of the dynamics. The method is extended to give an NPT ensemble simulation of hard sphere systems by applying an *ad hoc* rescaling of the velocities. The accuracy of the algorithms is tested by comparison with traditional NVE simulation results for the structural, thermodynamic, and transport properties.

DOI: 10.1103/PhysRevE.63.061106 PACS number(s): 02.70.Ns, 05.20.Jj

I. INTRODUCTION

Molecular dynamics (MD) simulations of hard sphere systems were first performed in the 1950s [1], and since then extensive simulation studies of this model have been performed, most notably by Alder and co-workers [2–5]. These simulations have revealed many useful insights into the molecular basis of thermodynamic and transport phenomena. Dynamics in hard sphere systems continues to interest researchers, with recent attention directed to dense packed metastable fluid states and crystallization processes [6–8].

While being among the simplest interaction potentials conceivable, the hard sphere potential provides a good approximation to phenomena in a large number of real materials. The comparison between hard sphere properties and those of systems with attractive as well as repulsive forces shows which effects are already brought about by repulsive interactions alone. This is especially the case for dense systems where the repulsive part of the interaction potential has a strong influence on the configurational properties and dynamics. Hard sphere system analysis revealed strong evidence for the existence of a first-order transition from an ordered to a disordered phase simply from short-range repulsions [9–12].

In recent work, dispersions of polymer coated colloidal particles have been investigated in which the behavior is extremely similar to that of hard sphere systems [13–17]. Such systems are not only exciting model systems for the analysis of crystallization processes, they are also of technological interest, for example for the production of photonic crystals [18]. The colloidal dispersions reproduce the hard sphere equation of state and exhibit a pressure-induced restructuring towards face-centered-cubic (fcc) order. Experimental investigations of these systems with their larger number of particles and the longer observation times are an ideal complement to the simulation studies, which for their part allow a more detailed structure analysis. Comparison of the two is a fruitful way to develop new insights in hard sphere system behavior.

Molecular dynamics simulations at constant pressure have become a standard method for the computational investigation of soft potential model systems [19,20]. One possible constant pressure scenario is the NPH ensemble, in which a system of N molecules in a fluctuating volume V is exposed to a constant pressure P at a constant enthalpy H. Corresponding NPH ensemble simulations for soft potentials are typically based on a method originally introduced by Andersen [21]. MD simulation techniques for hard sphere systems are computationally different from those for continuous model potentials because of the nature of the hard sphere collisions. While for soft molecules the numerical integration of the trajectory is typically performed by time steps of predetermined length, the propagation of hard sphere system simulations is event driven by the subsequential sphere collisions. For hard systems without external fields in the NVE ensemble, Newton's equations of motion can be integrated without truncation error because the collision dynamics can be evaluated analytically and the motion between collisions is force-free. Over the years, some efficiency improvements of the hard sphere MD method have been proposed [23,24], but generally it always consists of three fundamental steps: estimation of collision times, propagation of the system towards the next collision event, and calculation of the collision's impact on the system. If hard sphere simulations are carried out in the NPH ensemble, the system's volume is considered as an additional dynamical variable and all three simulation steps must be reconsidered.

In 1986, de Smedt *et al.* [22] presented the analysis necessary to implement the Andersen algorithm for hard sphere systems in ν dimensions together with some illustrative calculations for the one-dimensional case. However, to the best of our knowledge no implementation of their analysis for three-dimensional hard sphere systems has been reported up to now. Isobaric molecular dynamics is a potentially useful approach to studying the dynamics of hard sphere crystallization, so an implementation is of significant interest. In the present paper, the necessary steps for an efficient implementation in three dimensions are presented together with illustrative calculations. The accuracy of hard sphere NPH simulations is checked by comparison with results from NVE simulations. We also study the accuracy of simulations in which a simple velocity scaling is added to the algorithm to enable isothermal, isobaric (NPT), hard sphere simulations. In Sec. II, the derivation of the equations of motion for the hard sphere NPH ensemble is given. Section III is dedicated to implementation details, while tests of the algorithm are

reported in Sec. IV. In Sec. V, our conclusions are presented.

II. EQUATIONS OF MOTION FOR HARD SPHERES IN THE *NPH* ENSEMBLE

A. Molecular dynamics in the *NPH* ensemble

In the *NPH* ensemble, a system of N molecules in a fluctuating volume, V, is exposed to a constant external pressure P_E at a constant enthalpy $H=U+P_EV$, where U is the internal energy. The present paper is restricted to systems of spherical molecules where the configurational potential energy, $U(\ldots,\mathbf{r}_i,\ldots)$, is a function of the center-of-mass coordinates, $\mathbf{r}_i$, only. The molecules with masses m_i are assumed to be located within a cubic cell where periodic boundary conditions are imposed. In the following, the terms ''molecule'' and ''sphere'' are used synonymously.

NPH ensemble simulations are typically based on the Andersen method [21] in which the system is characterized by the scaled coordinates

$$\mathbf{q}_i=V^{-1/3}\mathbf{r}_i \tag{2.1}$$

and the volume V is an additional variable. By definition, the scaled coordinates $\mathbf{q}_i$ are located within the unit cube. The Andersen's Lagrangian is defined as

$$L=\frac{V^{2/3}}{2}\sum_{i=1}^{N} m_i\dot{\mathbf{q}}_i\cdot\dot{\mathbf{q}}_i-U(\ldots,V^{1/3}\mathbf{q}_i,\ldots)+\tfrac{1}{2}M\dot{V}^2-P_EV, \tag{2.2}$$

where M is a system parameter, which influences the dynamics of the volume change. The Lagrangian equations of motion are then given by

$$m_i\ddot{\mathbf{q}}_i=-V^{-2/3}\boldsymbol{\nabla}_{\mathbf{q}_i}U-2m_i\dot{\mathbf{q}}_i\frac{\dot{V}}{3V}, \tag{2.3}$$

$$M\ddot{V}=\frac{1}{3V^{1/3}}\sum_i m_i\dot{\mathbf{q}}_i^2-\frac{\partial U}{\partial V}-P_E. \tag{2.4}$$

In their article, de Smedt *et al.* [22] describe how to adapt the Andersen algorithm to a ν-dimensional system of hard spheres. For convenience, we present the essential steps in their derivation for the three-dimensional case. Although in Sec. IV only one-component systems are considered, the more general case of a hard sphere mixture with individual masses m_i and diameters σ_i is assumed.

B. Collision of hard spheres in the *NPH* ensemble

In a hard sphere system, the pair interaction potential of molecules i and j having a distance r is given by

$$u(r)=\begin{cases}\infty, & r<\sigma\\ 0, & r\geqslant\sigma,\end{cases} \tag{2.5}$$

where $\sigma=\frac{1}{2}(\sigma_i+\sigma_j)$. The dynamics of a hard sphere system at constant volume consists of time intervals of force-free motion interrupted by instantaneous two-molecule collisions. The collision behavior in the *NPH* ensemble can be analyzed by defining a soft interaction potential

$$u_\epsilon(r)=\begin{cases}\dfrac{\sigma-r}{\epsilon}, & r<\sigma\\ 0, & r\geqslant\sigma,\end{cases} \tag{2.6}$$

which becomes the hard sphere interaction potential in the limit $\epsilon\to0$. Using vectors $\mathbf{Q}=(m_j\mathbf{q}_j+m_i\mathbf{q}_i)/(m_i+m_j)$ and $\mathbf{q}:=\mathbf{q}_j-\mathbf{q}_i$ in analogy to center-of-mass vector and distance vector and introducing spherical coordinates (q,ϑ,φ) for the vector $\mathbf{q}$, the Lagrangian L_2 for two molecules can be written as

$$L_2=\frac{m_i+m_j}{2}V^{2/3}\dot{\mathbf{Q}}^2+\frac{\mu}{2}V^{2/3}[\dot{q}^2+q^2\dot{\vartheta}^2+q^2(\sin^2)\vartheta\dot{\varphi}^2)]$$
$$-u_\epsilon(V^{1/3}q)+\frac{M}{2}\dot{V}^2-P_EV, \tag{2.7}$$

where $\mu=(m_im_j)/(m_i+m_j)$ is the reduced mass. For finite ϵ, the collision takes place in the time interval $(0,t_d)$ in which the distance between the molecules $r=V^{1/3}q$ is less than σ. During the collision, the equations of motion for q and V are given by

$$\ddot{q}=q\dot{\vartheta}^2+q(\sin^2\vartheta)\dot{\varphi}^2-2\frac{\dot{V}}{3V}\dot{q}+\frac{1}{\mu V^{1/3}\epsilon} \tag{2.8}$$

and

$$\ddot{V}=\frac{m_i+m_j}{3MV^{1/3}}\dot{\mathbf{Q}}^2+\frac{\mu}{3MV^{1/3}}[\dot{q}^2+q^2\dot{\vartheta}^2+q^2(\sin^2)\vartheta\dot{\varphi}^2]$$
$$+\frac{q}{3MV^{2/3}\epsilon}-P_E. \tag{2.9}$$

As $\epsilon\to0$, the potential approaches the hard sphere limit and so the acceleration on the left-hand side of Eq. (2.8) diverges. The variables ϑ, φ, q, and V will remain finite as well as their derivatives $\dot{\vartheta}$, $\dot{\varphi}$, $\dot{q}$, and $\dot{V}$. Thus, while the left-hand side goes to infinity for $\epsilon\to0$, on the right-hand side the only term that increases unboundedly is $(\mu V^{1/3}\epsilon)^{-1}$. For this reason, the other terms may be neglected for sufficiently small ϵ and Eq. (2.8) becomes

$$\epsilon\ddot{q}=\frac{1}{\mu V^{1/3}} \tag{2.10}$$

while with an analogous argument Eq. (2.9) becomes

$$\epsilon\ddot{V}=\frac{q}{3MV^{2/3}}. \tag{2.11}$$

The remaining variables are unaffected by the hard sphere collision process. We consider a collision starting at $t=0$. For a small enough ϵ, the duration of the collision becomes

so small that during the collision $q(t)$ and $V(t)$ are accurately described by a Taylor expansion in t:

$$q(t) \approx q(0) + \dot{q}(0)t + \frac{t^2}{2\mu V^{1/3}(0)\epsilon}, \tag{2.12}$$

$$V(t) \approx V(0) + \dot{V}(0)t + \frac{\sigma t^2}{6MV(0)\epsilon}. \tag{2.13}$$

The collision duration is determined by the interval between the times $t=0$ and $t=t_d>0$ at which $r=V^{1/3}q=\sigma$:

$$V^{1/3}(t_d)q(t_d) = \sigma = V^{1/3}(0)q(0). \tag{2.14}$$

While the collision duration goes to zero for $\epsilon \to 0$, the value $\overline{t}_d = t_d/\epsilon$ remains finite. Equations (2.12) and (2.13) can be rewritten as

$$q(t) \approx q(0) + \epsilon \left\{ \dot{q}(0)\overline{t} + \frac{\overline{t}^2}{2\mu V^{1/3}(0)} \right\}, \tag{2.15}$$

$$V(t) \approx V(0) + \epsilon \left\{ \dot{V}(0)\overline{t} + \frac{\sigma \overline{t}^2}{6MV(0)} \right\}. \tag{2.16}$$

For small ϵ we may neglect all terms of the order ϵ^2 and higher so that combining Eqs. (2.14)–(2.16) gives

$$\begin{aligned} 0 &= V(t_d)q^3(t_d) - V(0)q^3(0) \\ &\approx \epsilon \overline{t}_d \left\{ [q^3(0)\dot{V}(0) + 3V(0)q^2(0)\dot{q}(0)] \right. \\ &\quad \left. + \left[q^3(0)\frac{\sigma}{6MV(0)} + \frac{3V(0)q^2(0)}{2\mu V^{1/3}(0)} \right] \overline{t}_d \right\}. \end{aligned} \tag{2.17}$$

The curly bracket becomes zero if

$$\overline{t}_d = -\frac{2\mu \left[V^{1/3}(0)\dot{q}(0) + \sigma \frac{\dot{V}(0)}{3V(0)} \right]}{1 + \frac{\mu\sigma^2}{9MV^2(0)}}. \tag{2.18}$$

For $\epsilon \to 0$, it follows from Eqs. (2.15) and (2.16) that V and q remain unchanged during a hard sphere collision while their derivatives change discontinuously as expected:

$$\dot{q}(t_d) = \dot{q}(0) + \frac{\overline{t}_d}{\mu V^{1/3}(0)}, \tag{2.19}$$

$$\dot{V}(t_d) = \dot{V}(0) + \frac{\sigma \overline{t}_d}{3MV(0)}. \tag{2.20}$$

Finally, one has

$$\Delta \dot{\mathbf{q}}_j = \frac{\overline{t}_d}{m_j \sigma}\mathbf{q}, \qquad \Delta \dot{\mathbf{q}}_i = -\frac{\overline{t}_d}{m_i \sigma}\mathbf{q}, \tag{2.21}$$

$$\Delta \dot{V} = \frac{\sigma \overline{t}_d}{3MV}, \tag{2.22}$$

$$\overline{t}_d = -\frac{2\mu \left[V^{1/3}\dot{q}^b + \sigma \frac{\dot{V}^b}{3V} \right]}{1 + \frac{\mu\sigma^2}{9MV^2}}, \tag{2.23}$$

$$\dot{q}^b = \sigma^{-1} V^{1/3} (\dot{\mathbf{q}}_j^b - \dot{\mathbf{q}}_i^b) \cdot \mathbf{q}, \tag{2.24}$$

where $\dot{\mathbf{q}}_i^b$, $\dot{\mathbf{q}}_j^b$, and $\dot{V}_b$ are the respective values before the collision and $\mathbf{q} = \mathbf{q}_j - \mathbf{q}_i$.

C. Motion between collisions

Between collisions, the path of the molecules and the change of the volume are given by the set of $3N+1$ differential equations:

$$m_i \ddot{\mathbf{q}}_i = -2m_i \dot{\mathbf{q}}_i \frac{\dot{V}}{3V} \qquad (i = 1, \ldots, N), \tag{2.25}$$

$$M\ddot{V} = \frac{1}{3V^{1/3}} \sum_i m_i \dot{\mathbf{q}}_i^2 - P_E. \tag{2.26}$$

Multiplying Eq. (2.25) with $\dot{\mathbf{q}}_i$ and summing over all i gives

$$\dot{\chi} = -\frac{4}{3}\chi \frac{\dot{V}}{V}, \tag{2.27}$$

where

$$\chi = \sum_i \frac{m_i}{2} \dot{\mathbf{q}}_i^2 \tag{2.28}$$

is related to the molecules' kinetic energy, K_{mol}, by $K_{\mathrm{mol}} = V^{2/3}\chi$. Note that for the total kinetic energy, K, the contribution from the volume dynamics must be added, $K = K_{\mathrm{mol}} + M\dot{V}^2/2$. The solution of Eq. (2.27) is

$$\chi(t) = CV^{-4/3}(t)$$

$$\text{with} \quad C := \chi(t_0)V^{4/3}(t_0) = K_{\mathrm{mol}}(t_0)V^{2/3}(t_0). \tag{2.29}$$

Thus, in the NPH ensemble, the hard spheres' kinetic energy $K_{\mathrm{mol}}(t)$ is generally not a constant between two collisions. Instead we find that

$$\frac{K_{\mathrm{mol}}(t)}{K_{\mathrm{mol}}(t_0)} = \left(\frac{V(t)}{V(t_0)} \right)^{-2/3}. \tag{2.30}$$

Substituting Eq. (2.29) into Eq. (2.26) gives

$$\ddot{V}(t) = \frac{2C}{3M} V^{-5/3}(t) - \frac{P_E}{M}. \tag{2.31}$$

As expected, the equation of state for the ideal gas

$$\tfrac{2}{3}K = P_E V \tag{2.32}$$

is a solution of Eq. (2.31) in the special case of $\dot{V}=0$. In the next section, we describe some aspects of the implementation, especially the dynamics between collisions. The full algorithm is given in Appendix A.

III. IMPLEMENTATION

The equations of motion for the hard spheres depend on the dynamics of the volume, which is determined by Eq. (2.31). Equation (2.31) can be transformed into a first-order differential equation. In this way, an integral expression for the inverse function $t(V^{1/3})$ can be found that solves Eq. (2.31). The integral cannot, however, be solved analytically. Nevertheless, a numerical integration of Eq. (2.31) itself is quite convenient, particularly for the purpose of estimating the collision times.

A. Integration method for small time steps

For small time steps, $\tilde{t}=t-t_0$, Eq. (2.31) can be solved numerically by a method similar to the Velocity-Verlet algorithm [19],

$$\begin{aligned} V(t) &\approx V(t_0)+\dot{V}(t_0)\tilde{t}+\tfrac{1}{2}\ddot{V}(t_0)\tilde{t}^2, \\ \dot{V}(t) &\approx \dot{V}(t_0)+\tfrac{1}{2}\tilde{t}[\ddot{V}(t_0)+\ddot{V}(t)]. \end{aligned} \tag{3.1}$$

The second derivative of V is given by Eq. (2.31). Defining $V_0=V(t_0)$, $V_1=V(t)$, $\dot{V}_0=\dot{V}(t_0)$, and $\dot{V}_1=\dot{V}(t)$, we obtain

$$\begin{aligned} V_1 &= V_0+\dot{V}_0\tilde{t}+(\zeta V_0^{-5/3}-\eta)\tilde{t}^2, \\ \dot{V}_1 &= \dot{V}_0+[(\zeta V_0^{-5/3}-\eta)+(\zeta V_1^{-5/3}-\eta)]\tilde{t}, \end{aligned} \tag{3.2}$$

where $\zeta=C/3M$ and $\eta=P_E/2M$. From Eq. (2.25), one has

$$\dot{\mathbf{q}}_i(t)=\boldsymbol{\kappa}_i V^{-2/3}(t), \quad \text{with} \quad \boldsymbol{\kappa}_i=\dot{\mathbf{q}}_i(t_0)V^{2/3}(t_0). \tag{3.3}$$

For small $\tilde{t}$, the scaled coordinates $\mathbf{q}_i^1=\mathbf{q}_i(t)$ and their time derivatives $\dot{\mathbf{q}}_i^1=\dot{\mathbf{q}}_i(t)$ are given by

$$\begin{aligned} \mathbf{q}_i^1 &\approx \mathbf{q}_i^0+\dot{\mathbf{q}}_i^0\tilde{t}+\tfrac{1}{2}\ddot{\mathbf{q}}_i(t_0)\tilde{t}^2=\mathbf{q}_i^0+\dot{\mathbf{q}}_i^0\tilde{t}-\dot{\mathbf{q}}_i^0\frac{\dot{V}_0}{3V_0}\tilde{t}^2, \\ \dot{\mathbf{q}}_i^1 &= V_1^{-2/3}\boldsymbol{\kappa}_i, \\ \boldsymbol{\kappa}_i &= V_0^{2/3}\dot{\mathbf{q}}_i^0, \end{aligned} \tag{3.4}$$

where $\mathbf{q}_i^0=\mathbf{q}_i(t_0)$ and $\dot{\mathbf{q}}_i^0=\dot{\mathbf{q}}_i(t_0)$.

B. Estimating the next collision time

The next step is to develop a method to calculate the time when the next hard sphere collision will occur. With this knowledge and using the equations from Sec. IV B, the system can be propagated up to that time. The collision time must be calculated for every pair of molecules, which are close enough to be a candidate for the next collision. A pair of molecules is considered a candidate for a collision if r is less than some suitably chosen value, the choice of which is discussed below. The earliest of the obtained collision times, $\{t_c\}$, is the time of the next collision. The condition for a collision between molecules i and j is

$$V^{2/3}(t_c)|\mathbf{q}_{ij}|^2(t_c)=\sigma^2 \tag{3.5}$$

with $\mathbf{q}_{ij}=\mathbf{q}_j-\mathbf{q}_i$. Using the notations

$$\begin{aligned} &q_0^2=|\mathbf{q}_{ij}(t_0)|^2, \quad \dot{q}_0^2=|\dot{\mathbf{q}}_{ij}(t_0)|^2, \quad \mathbf{q}_i^0=\mathbf{q}_i(t_0), \\ &J_0:=\frac{\dot{V}_0}{3V_0}, \quad s_0:=2[\mathbf{q}_{ij}(t_0)\cdot\dot{\mathbf{q}}_{ij}(t_0)], \quad \hat{t}:=t-t_0, \end{aligned} \tag{3.6}$$

one obtains

$$|\mathbf{q}_{ij}|^2(t)\approx q_0^2+s_0(\hat{t}-J_0\hat{t}^2)+\dot{q}_0^2(\hat{t}-J_0\hat{t}^2)^2. \tag{3.7}$$

For small time differences $\hat{t}$, a Taylor expansion of $V^{2/3}(t)|\mathbf{q}_{ij}|^2(t)$ results in

$$\begin{aligned} &V^{2/3}(t)|\mathbf{q}_{ij}|^2(t) \\ &\approx V^{2/3}(t_0)|\mathbf{q}_{ij}|^2(t_0)+\frac{d}{dt}[V^{2/3}|\mathbf{q}_{ij}|^2]_{t_0}\hat{t} \\ &\quad+\frac{1}{2}\frac{d^2}{dt^2}[V^{2/3}|\mathbf{q}_{ij}|^2]_{t_0}\hat{t}^2 \\ &= V_0^{2/3}\Bigg\{q_0^2+(2J_0q_0^2+s_0)\hat{t}+\Bigg[\frac{2}{3}V_0^{-1}q_0^2(\zeta V_0^{-5/3}-\eta) \\ &\quad-J_0^2q_0^2+J_0s_0+\dot{q}_0^2\Bigg]\hat{t}^2\Bigg\} \\ &= \sigma^2 \quad \text{for} \quad t=t_c. \end{aligned} \tag{3.8}$$

Rearranging this gives the quadratic equation

$$u\hat{t}_c^2+v\hat{t}_c+w=0, \tag{3.9}$$

where

$$u=\left[\frac{2}{3}V_0^{-1}q_0^2(\zeta V_0^{-5/3}-\eta)-J_0^2q_0^2+J_0s_0+\dot{q}_0^2\right], \tag{3.10}$$

$$v=(2J_0q_0^2+s_0), \tag{3.11}$$

and

$$w=q_0^2-\frac{\sigma^2}{V_0^{2/3}}. \tag{3.12}$$

It follows that if $(v^2/4u^2)-(w/u)>0$, then molecules i and j collide at

$$\hat{t}_c=t_c-t_0=-\frac{v}{2u}\pm\sqrt{\frac{v^2}{4u^2}-\frac{w}{u}}. \tag{3.13}$$

Taking the negative sign with the square root gives the smallest value for $\hat{t}_c$ in each case. In molecular dynamics simulations in the NVE ensemble, possible colliders are characterized by $\mathbf{r}_{ij}\cdot\dot{\mathbf{r}}_{ij}<0$; for them, both values of $\hat{t}_c$ are positive and the smaller $\hat{t}_c$ is always the correct collision time if the collision is not hindered by third molecules. In the NPH ensemble, the time dependence of the volume may lead to configurations where Eq. (3.13) has both negative and positive solutions, in which case the latter determines the relevant future collision time. Thus the collision time is the smallest positive solution of Eq. (3.13) if any positive solution exists. This strategy presumes that the molecules in question are not overlapping. Therefore, small overlaps due to numerical inaccuracy must be carefully corrected. To avoid systematic drifts in the enthalpy, one consequently rectifies any deviations from the contact distance for the actually colliding spheres. If the deviations are small enough, it is sufficient to rectify the colliders' positions only.

IV. SOME TESTS OF THE ALGORITHM

We have tested the algorithm described above for one-component hard sphere systems in the NPH ensemble and compared the results with simulations performed in the NVE ensemble.

A. Simulation details

Test runs were performed in a cubic simulation box with periodic boundary conditions. At the beginning, the spheres were located on the sites of an fcc lattice. While the diameter of the spheres serves as a suitable unit of length, no corresponding reference energy is provided by the hard sphere potential. For hard spheres in the NVE ensemble, the kinetic energy and temperature are (arbitrary) constants since the potential energy is zero for nonoverlapping configurations of the spheres. In the NPH ensemble, the temperature T, determined by

$$\frac{3(N-1)+1}{2}kT=\sum_{i=1}^{N}\frac{m_i}{2}V^{2/3}\dot{\mathbf{q}}_i^2+\frac{M}{2}\dot{V}^2, \tag{4.1}$$

is a fluctuating quantity. We have found it convenient to use kT_0 as the unit of energy with T_0 being the initial temperature.

Usually the properties of hard sphere systems are plotted in terms of dimensionless density, $\rho^*=\rho\sigma^3=N\sigma^3/V$, and the dimensionless ratio of pressure and temperature $(P_E/kT)^*=P_E\sigma^3/kT$. However, while $\rho\sigma^3$ is constant in the NVE ensemble, neither $\rho\sigma^3$ nor $P_E\sigma^3/kT$ are constant in the NPH ensemble where V and T are fluctuating. Since in the NPH ensemble the enthalpy H is constant, one has

$$H=E+P_EV=\frac{3N-2}{2}kT+P_EV=\text{const.} \tag{4.2}$$

For large N, H/NP_E can be written as

$$\frac{H}{NP_E}=\frac{3}{2}\left(\frac{P_E}{kT}\right)^{-1}+\rho^{-1}. \tag{4.3}$$

Equation (4.3) gives a relation between the fluctuating quantities P_E/kT and ρ. In the $(P_E/kT,\rho)$ plane, the system fluctuates along a hyperbolic curve that is determined by the constant $H/(NP_E)$ on the left-hand side of Eq. (4.3). The curves for different $H/(NP_E)$ do not intersect. If we write Eq. (4.3) in the form

$$\frac{H}{P_E}-\frac{3Nk}{2P_E}T=V, \tag{4.4}$$

then it follows that in the NPH ensemble of hard spheres, changes of the volume are proportional to changes of the temperature, i.e.,

$$\Delta V=-\frac{3Nk}{2P_E}\Delta T, \tag{4.5}$$

a decrease of the volume implying an increase of the temperature and vice versa.

The hard sphere molecular dynamics simulations were run for systems with $N=864$, 2048, and 10 976 spheres over a reduced time period of $t^*=10^2-10^3$, including up to 10^8 collisions. The reduced time t^* is defined by $t^*=t/(\sigma\sqrt{m/kT_0})$

B. NPT ensemble simulations

It is an interesting question how the algorithm should be modified to perform NPT simulations of hard spheres. The NPT ensemble has a number of advantages compared to the NPH ensemble. In experiments, typically the temperature is kept constant rather than the enthalpy so that an NPT simulation may be more adequate to mimic the dynamics in the experiment. As mentioned in Sec. IV A, the NPH ensemble for hard spheres also has some conceptual inconveniences: For hard sphere systems in the NPH ensemble, neither $\rho\sigma^3$ nor $P_E\sigma^3/kT$ are constant since volume fluctuations are accompanied by proportional fluctuations of the temperature. It follows from Eq. (4.3) that there is a minimum density that can be encountered in a hard sphere dynamics in the NPH ensemble for a given value of H/NP_E. This is given by

$$\rho_{\min}=\frac{NP_E}{H}. \tag{4.6}$$

This behavior is illustrated in Fig. 1, which shows the hard sphere equation of state together with the curves obtained from Eq. (4.3) for various values of H/NP_E. It follows that the solid branch cannot be reached if the density of the initial configuration is chosen too low. For example, at the melting point of the solid, for which $P_E\sigma^3/kT\approx 11.59$ and $\rho\sigma^3\approx 1.041$, we have

$$\frac{H}{NP_E}\approx 1.09\sigma^3=\frac{1}{0.92}\sigma^3. \tag{4.7}$$

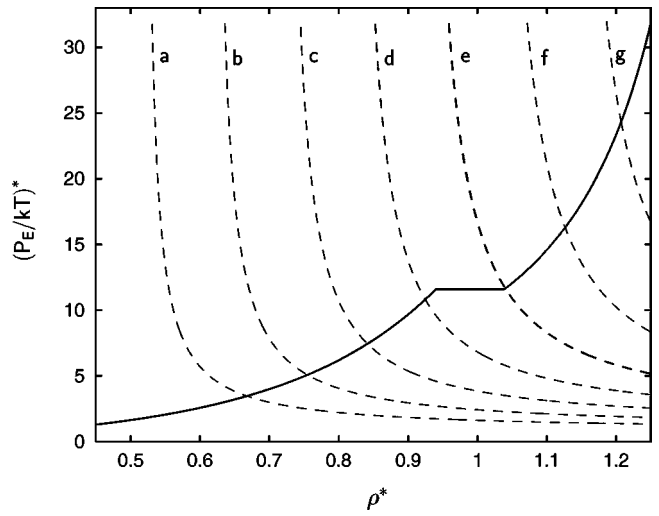

FIG. 1. Equation of state for hard spheres (solid line) in the fluid phase (from the Carnahan-Starling equation [26]) and solid phase (from the Hall equation [27]) together with plots from Eq. (4.3) (dashed lines) for $H/(NP_E\sigma^3)=$: (a) 1.93; (b) 1.62; (c) 1.39; (d) 1.22; (e) 1.09; (f) 0.98; (g) 0.89. The thick dashed parabolic line (e) passes through the melting point.

Thus, neither the melting solid nor any solid state with a higher density can be reached from an initial fluid state with a density $\rho\sigma^3<0.92$ using the dynamics of the NPH ensemble. Generally, crystallization processes have to start from fluid states with sufficiently high densities and typically rather high values for $P_E\sigma^3/kT$. These problems disappear in the NPT ensemble where $P_E\sigma^3/kT$ is constant. To obtain hard sphere dynamics in this ensemble, we could, in principle, start with the Lagrangian equations introduced by Nosé [25] and derive in a straightforward procedure the equations of motion and the collision behavior. The expressions describing the collision behavior turn out to be very similar to those in the NPH ensemble. However, the equations of motion between collisions are more complex than those for the NPH case, and they would require a more accurate predictor corrector algorithm than the one we have implement in the NPH case. This makes the estimate of the next collision event distinctly more CPU time-consuming. Simulations with sufficiently extensive system sizes and long runs would not be practical. As an alternative to this, we have implemented a rescaling technique in which after each propagation step the hard sphere velocities and the time derivative of the volume are rescaled such that

$$\text{const}=kT=\frac{2}{3(N-1)+1}\left(\sum_{i=1}^{N}\frac{m_i}{2}V^{2/3}\dot{\mathbf{q}}_i^2+\frac{M}{2}\dot{V}^2\right). \tag{4.8}$$

Since in the NPT ensemble the temperature is constant, kT can be taken to define an energy reference unit. Although this procedure does not yield rigorous NPT molecular dynamics, we shall see that the results obtained for thermodynamics and transport properties are in good agreement with those obtained from rigorous NVE and NPH dynamics.

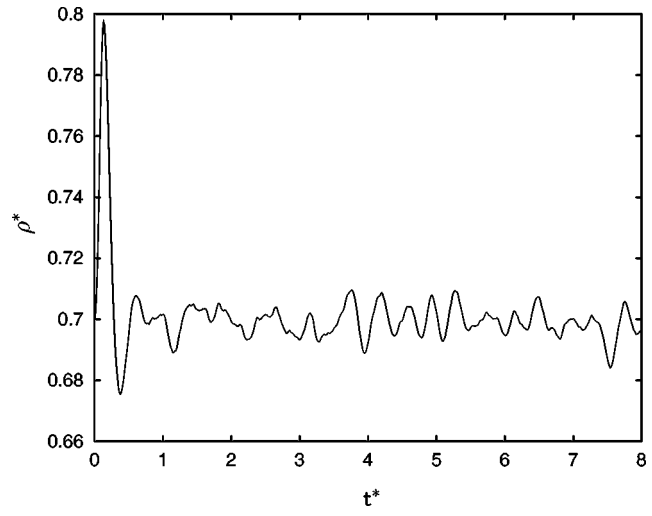

FIG. 2. Reduced density $\rho\sigma^3$ as a function of reduced time $t^*=t\sqrt{kT_0/(m\sigma^2)}$ at the beginning of an NPH simulation with $P_E\sigma^3/kT_0=4.0$.

C. System dynamics

The maximum time step must be small enough to produce tolerable errors in the estimation of the next collision time. At the moment of collision, the distance $r_{ij}(t_c)$ of colliding spheres i and j should be σ_{ij}. For time steps smaller than $\tilde{t}_{\max}=10^{-4}$, the deviations were never larger than $2\times10^{-8}\sigma_{ij}$. For high densities the problem is less important since the estimated time steps $\tilde{t}_c$ towards the next collision are already so small that no intermediate step is required.

There is no precise rule to choose the order of magnitude for the value M which controls the dynamics of the volume V. The choice of M does not influence any equilibrium properties but it has an impact on the dynamics. As a rule of thumb, Andersen [21] proposed that the time scale of the volume fluctuation should be approximately the length of the sample divided by the speed of sound in the sample. For a cubic system with 2048 atoms, the fluctuation time scale should be of the order of $0.1-1.0$ in reduced units. Large values of M lead to slow, periodic volume oscillations, while a small value of M results in fast irregular fluctuations of V. In the latter case, the dynamics of the volume is mainly driven by the molecular collisions rather than by the inertia of an artificial piston. The volume dynamics is dependent on the density of the system. However, for all densities $\rho\sigma^3\geqslant0.4$ a value of $M^*=10^{-4}$ turns out to be reasonable in terms of the mentioned criteria. If a simulation starts close to an equilibrium state point with $\dot{V}=0$, the system typically undergoes one or two larger oscillations in density and temperature until it rapidly approaches its longtime fluctuating behavior (see Fig. 2).

An important criterion for the accuracy of NPH simulations is the conservation of enthalpy. In our test simulations, we found that the enthalpy never deviated more than 0.005% from its initial value over the course of the run.

D. Equilibrium properties

A number of test simulations were performed to check the accuracy of the system's equilibrium properties. Results

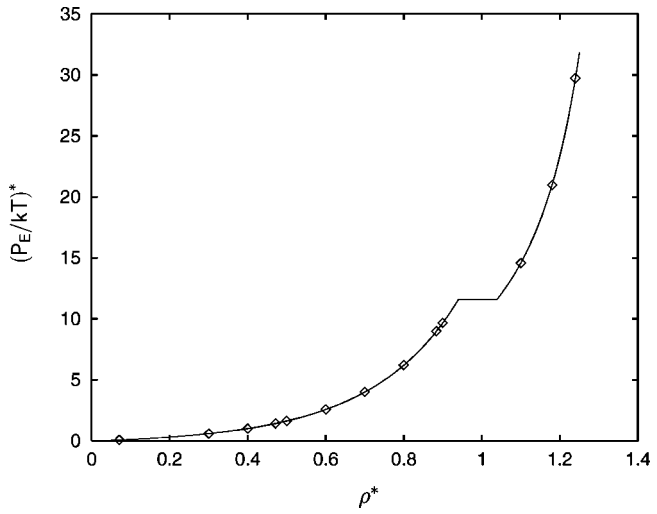

FIG. 3. Equation of state for hard spheres in the fluid and solid phases. *NPH* simulation results ($\diamond$) of the average reduced pressure over temperature $\langle (P_E/kT)\rangle\sigma^3$ as a function of the average reduced density $\langle\rho\rangle\sigma^3$ are shown. The values are obtained from independent runs with different pressure parameter values. The solid lines represent the Carnahan-Starling equation for the fluid phase for $\rho\sigma^3<0.943$ and the equation of state for hard sphere fcc solids proposed by Hall [27] for $\rho\sigma^3>1.041$.

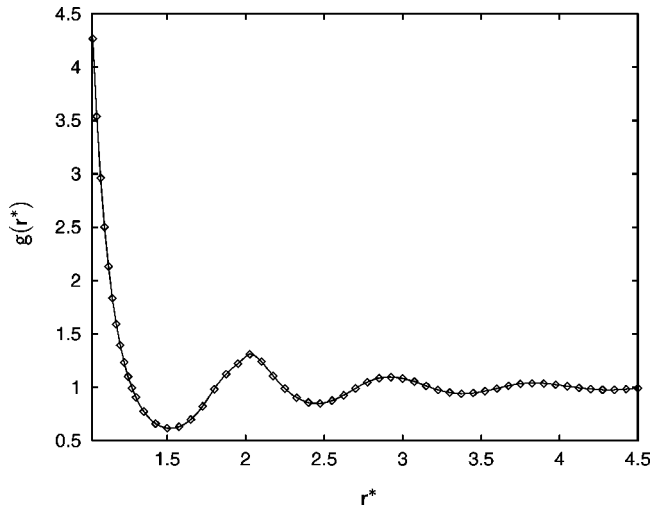

FIG. 4. Pair distribution function from *NPH* (solid line) and *NVE* ($\diamond$) ensemble simulations. *NPH* simulation results are shown for $\langle (P_E/kT)\rangle\sigma^3=9.6715$. *NVE* results refer to the corresponding state with the density of $\rho\sigma^3=0.9$. Only a subset of the *NVE* simulation values are drawn to leave the *NPH* curve visible.

were compared with accurate equations of state and corresponding *NVE* ensemble results. Figure 3 shows the equation-of-state data obtained. The lines in Fig. 3 correspond to the Carnahan-Starling equation [26] in the fluid region and the Hall [27] equation in the solid region, which have been shown to give very accurate descriptions of the hard sphere equation of state. The agreement is very good with deviations less than 0.2% for the density for all states considered. The same accuracy was obtained with *NPT* simulations. The local fluid structure was considered by comparing pair distribution functions from *NPH*, *NPT*, and *NVE* simulations for various densities. Deviations always lay within the range of the statistical errors. As an example, the pair distribution functions obtained from *NVE* simulations of a hard sphere fluid with a density $\rho\sigma^3=0.9$ and the corresponding *NPH* ensemble simulation with $\langle\rho\rangle\sigma^3=0.9$ are shown in Fig. 4.

E. Transport properties

Due to the modified dynamics in constant pressure simulations, transport properties are of special interest. We have calculated the mean-square displacement and the velocity autocorrelation functions for several fluid states. As an example, Fig. 5 shows the velocity autocorrelation functions of systems with $\rho\sigma^3=0.9$ and $\langle\rho\rangle\sigma^3=0.9$ in the *NVE* and *NPH* ensemble, respectively. The deviation is smaller than the statistical fluctuations. A corresponding comparison between *NPT* and *NVE* ensemble results is made in Fig. 6. Since the rescaling method does not yield the rigorous dynamics of the *NPT* ensemble, the good agreement between *NPT* and *NVE* velocity autocorrelations is a reassuring indicator for the accuracy of the method. Diffusion coefficients obtained from *NVE*, *NPH*, and *NPT* ensemble simulations are shown in Fig. 6 together with original results from Alder, Gass, and Wainwright [5] (Fig. 7). For the *NVE* and the *NPT* ensemble, the diffusion coefficient is given in reduced form $D^*=D/(\sigma\sqrt{kT/m})$. For the *NPH* ensemble, D^* is defined by $D^*=D/(\sigma\sqrt{kT_0/m})$ and we started with a configuration on the equilibrium branch so that $\langle T\rangle=T_0$ within the error range. The deviations between the D values from the *NVE*, *NPH*, and *NPT* ensemble simulations are of the order of 1% or less and the differences are not systematic.

V. CONCLUSIONS

We have implemented molecular dynamics simulations of hard sphere systems in the *NPH* ensemble. A detailed de-

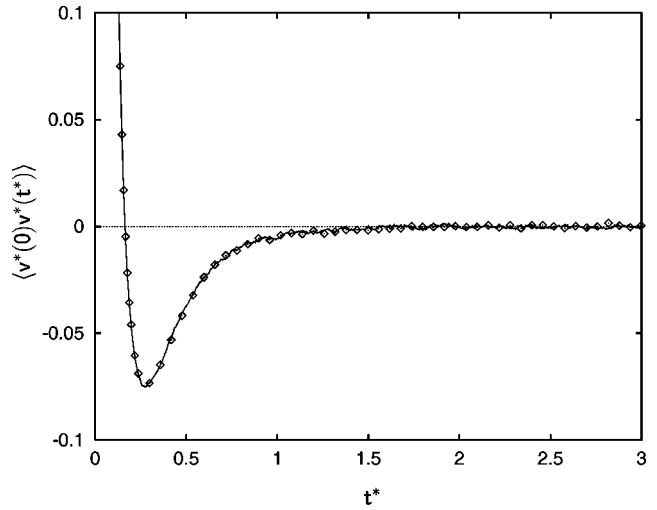

FIG. 5. Velocity autocorrelation function $\langle v^*(0)v^*(t^*)\rangle$ obtained from *NPH* (solid line) and *NVE* ($\diamond$) ensemble simulations. *NPH* simulation results are shown for $\langle (P_E/kT)\rangle\sigma^3=9.6715$. *NVE* results refer to the corresponding state with the density of $\rho\sigma^3=0.9$. Only a subset of the *NVE* simulation values are drawn to leave the *NPH* curve visible.

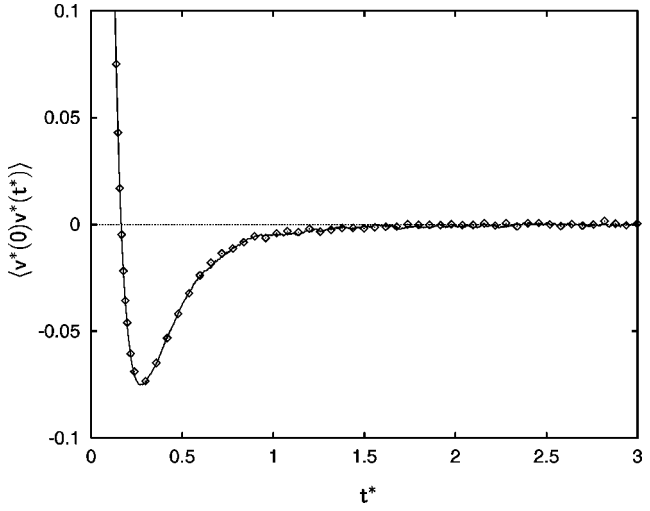

FIG. 6. Velocity autocorrelation function $\langle v^*(0)v^*(t^*)\rangle$ obtained from NPT (solid line) and NVE ($\diamond$) ensemble simulations. NPT simulation results are shown for $\langle (P_E/kT)\rangle\sigma^3=9.6715$. NVE results refer to the corresponding state with the density of $\rho\sigma^3=0.9$. Only a subset of the NVE simulation values are drawn to leave the NPT curve visible.

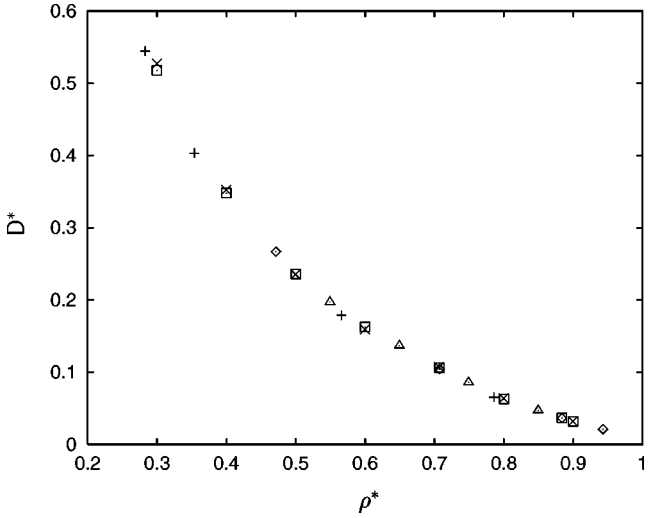

FIG. 7. The reduced diffusion coefficient $D^*=D\sqrt{m/kT_0}/\sigma$ obtained from the velocity autocorrelation function as a function of the reduced density $\rho\sigma^3$. Results are shown from simulations of Alder and Wainwright for $N=108$ (+) and for $N=500$ spheres ($\diamond$). The remaining results for the NPH ($\times$), the NPT ($\triangle$), and the NVE ($\square$) ensemble are obtained from simulations with $N=864$ spheres.

scription of the algorithm as well as technical details were presented. The algorithm described is based on the adaptation of the Andersen [21] method to hard spheres proposed by de Smedt and co-workers [22]. A key feature of our implementation is an efficient calculation of the dynamics between hard sphere collisions. Test comparisons with simulations carried out in the NVE ensemble demonstrate the accuracy of the NPH simulations. Test simulations were applied for the NPH ensemble algorithm and an NPT ensemble algorithm (based on ad hoc rescaling of the velocities) over the whole density range of the fluid phase as well as for the solid phase. Constant pressure simulations of hard sphere systems should be quite useful for the study of the dynamics at high pressures. By a one-step increase of the external pressure P_E, a quenching process can be mimicked. Up to now, quenches towards close-packed random systems required the application of rather sophisticated methods that are rather far from the system behavior in an experimental setup. The constant pressure simulations will allow us to analyze the system's immediate response on the quenching process. This will be the subject of a future publication.

ACKNOWLEDGMENTS

This work was supported by a grant from the U.S. Department of Energy (Contract No. DE-FG02-90ER14150). The authors are grateful to Professor Julian Talbot for providing us with a detailed explanation of the analysis presented in the paper by de Smedt *et al.* [22].

APPENDIX A: ALGORITHM

(i) At a certain time step t_0, the following values are assumed to be known:

(a) $\mathbf{q}_i^0$, $\dot{\mathbf{q}}_i^0$ and $\boldsymbol{\kappa}_i=\dot{\mathbf{q}}_i^0 V_0^{2/3}$ for all molecules i.

(b) V_0, $\dot{V}_0$, $\zeta=C/3M=(1/3M)V_0^{4/3}\Sigma_i(m_i/2)(\dot{\mathbf{q}}_i^0)^2$, $\eta=P_E/2M$, $J_0=\dot{V}_0/(3V_0)$, $A_0=(\zeta V_0^{-5/3}-\eta)$.

(ii) Calculate the collision time t_c for all reasonable pairs of molecules i and j:

$$u=\left[\frac{2}{3}V_0^{-1}q_0^2A_0-J_0^2q_0^2+J_0s_0+\dot{q}_0^2\right],$$

$$v=2J_0q_0^2+s_0,$$

$$w=q_0^2-\frac{\sigma^2}{V_0^{2/3}},$$

$$t_c=t_0-\frac{v}{2u}\pm\sqrt{\frac{v^2}{4u^2}-\frac{w}{u}}.$$

The smallest $t_c>t_0$ is the next collision time t_c^n. Neighbor lists help to reduce the number of possible colliders. It was found that a combination of a small radius neighbor shell ($r_{\text{shell}}=1.05\sigma$) and a segmentation of the simulation volume into cells leads to the best performance.

(iii) Determine the propagation time step $\tilde{t}=t_1-t_0$ so that it does not exceed the maximum time step $\tilde{t}_{\max}$ beyond which the Taylor approximations become questionable: i.e., set $\tilde{t}=\min\{t_c^n-t_0,\tilde{t}_{\max}\}$.

(iv) Propagate the system towards $t_1=t_0+\tilde{t}$:

(a) $V_1=V_0+\dot{V}_0\tilde{t}+A_0\tilde{t}^2$.

(b) Calculate V_1^{-1}, $V_1^{-2/3}$, $A_1=(\zeta V_0^{-5/3}-\eta)$, $J_1=\dot{V}_1/(3V_1)$.

(c) $\dot{V}_1=\dot{V}_0+(A_0+A_1)\tilde{t}$.

(d) $\mathbf{q}_i^1 = \mathbf{q}_i^0 + \dot{\mathbf{q}}_i^0(\tilde{t} - J_0\tilde{t}^2)$.

(e) $\dot{\mathbf{q}}_i^1 = V_1^{-2/3}\kappa_i$.

(v) If a collision occurs at t_1 between molecules i and j with $\mu = (m_i m_j)/(m_i + m_j)$, then do the following.

(a) Calculate

$$\mathbf{q} = \mathbf{q}_j - \mathbf{q}_i, \qquad \Delta\dot{\mathbf{q}}_j = \frac{\overline{t}_d}{m_j\sigma}\mathbf{q},$$

$$\dot{q}^b = \sigma^{-1}V^{1/3}(\dot{\mathbf{q}}_j^b - \dot{\mathbf{q}}_i^b)\cdot\mathbf{q}, \qquad \Delta\dot{\mathbf{q}}_i = -\frac{\overline{t}_d}{m_i\sigma}\mathbf{q},$$

$$\overline{t}_d = -\frac{2\mu\left[V^{1/3}\dot{q}^b + \sigma\dfrac{\dot{V}^b}{3V}\right]}{1 + \dfrac{\mu\sigma^2}{9MV^2}}, \qquad \Delta\dot{V} = \frac{\sigma\overline{t}_d}{3MV}.$$

(b) With $\dot{\mathbf{q}}_i^a = \dot{\mathbf{q}}_i^b + \Delta\dot{\mathbf{q}}_i$ and $\dot{\mathbf{q}}_j^a = \dot{\mathbf{q}}_j^b + \Delta\dot{\mathbf{q}}_j$ being the time derivatives of the $\mathbf{q}_i, \mathbf{q}_j$ before (b) and after (a) the collision, calculate

$$C^a = C^b + V_1^{4/3}\left[\frac{m_i}{2}[(\dot{\mathbf{q}}_i^a)^2 - (\dot{\mathbf{q}}_i^b)^2] + \frac{m_j}{2}[(\dot{\mathbf{q}}_j^a)^2 - (\dot{\mathbf{q}}_j^b)^2]\right].$$

(c) Set $\zeta^a = C^a/3M$, $A_a = (\zeta_a V_0^{-5/3} - \eta)$, and $J_a = \dot{V}_a/(3V_1)$.

(d) $\kappa_i = \dot{\mathbf{q}}_i^a V_1^{2/3}$, $\kappa_j = \dot{\mathbf{q}}_j^a V_1^{2/3}$

(vi) Set the following:

(a) $\mathbf{q}_i^0 = \mathbf{q}_i^1$, $\dot{\mathbf{q}}_i^0 = \dot{\mathbf{q}}_i^a$ for all molecules i.

(b) $V_0 = V_1$, $\dot{V}_0 = \dot{V}_a$, $\zeta = \zeta^a$, $J_0 = J_a$, $A_0 = A_a$.

(vii) Continue with step (ii).

[1] B.J. Alder and T.E. Wainwright, J. Chem. Phys. **27**, 1208 (1957).

[2] B.J. Alder and T.E. Wainwright, J. Chem. Phys. **31**, 459 (1959).

[3] B.J. Alder and T.E. Wainwright, Phys. Rev. **127**, 359 (1962).

[4] B.J. Alder and T.E. Wainwright, Phys. Rev. A **1**, 18 (1970).

[5] B.J. Alder, D.M. Gass, and T.E. Wainwright, J. Chem. Phys. **53**, 3813 (1970).

[6] M.D. Rintoul and S. Torquato, Phys. Rev. Lett. **77**, 4198 (1996).

[7] T.M. Truskett, S. Torquato, S. Sastry, P.G. Debenedetti, and F.H. Stillinger, Phys. Rev. E **58**, 3083 (1998).

[8] T.M. Truskett, S. Torquato, and P.G. Debenedetti, Phys. Rev. E **62**, 993 (2000).

[9] W.G. Hoover and F.H. Ree, J. Chem. Phys. **47**, 4873 (1967).

[10] W.G. Hoover and F.H. Ree, J. Chem. Phys. **49**, 3609 (1968).

[11] H. Reiss and A.D. Hammerich, J. Phys. Chem. **90**, 6252 (1986).

[12] P.A. Monson and D.A. Kofke, Adv. Chem. Phys. **115**, 113 (2000).

[13] M.A. Rutgers *et al.*, Phys. Rev. B **53**, 5043 (1996).

[14] Y.M. He, B.J. Ackerson, and W. van Megen, Phys. Rev. E **54**, 5286 (1996).

[15] M.S. Elliot, B.T.F. Bristol, and W.C.K. Poon, Physica A **235**, 216 (1997).

[16] C. Dux and H. Versmold, Phys. Rev. Lett. **78**, 1811 (1997).

[17] J.L. Harland and W. van Megen, Phys. Rev. E **55**, 3054 (1997).

[18] R.M. Amos, T.J. Shepherd, J.G. Rarity, and P. Tapster, Electron. **36**, 1411 (2000).

[19] M.P. Allen and D.J. Tildesley, *Computer Simulation of Liquids* (Clarendon Press, Oxford, 1987).

[20] D. Frenkel and B. Smit, *Understanding Molecular Simulation* (Academic Press, San Diego, 1996).

[21] H.C. Andersen, J. Chem. Phys. **72**, 2384 (1980).

[22] Ph. de Smedt, J. Talbot, and J.L. Lebowitz, Mol. Phys. **59**, 625 (1986).

[23] B.D. Lubachevsky, J. Comput. Phys. **94**, 255 (1991).

[24] M. Marín, D. Risso, and P. Cordero, J. Comput. Phys. **109**, 306 (1993).

[25] S. Nosé, J. Chem. Phys. **81**, 511 (1984).

[26] N.F. Carnahan and K.E. Starling, J. Chem. Phys. **51**, 635 (1969).

[27] K.R. Hall, J. Chem. Phys. **57**, 2252 (1970).